

Supplementary Information

Experimental design, validation and computational modeling uncover DNA damage sensing by DNA-PK and ATM

Robert J Flassig^{*1}, Gunter Maubach², Christian Träger², Kai Sundmacher^{1,3} and
Michael Naumann²

¹Max Planck Institute for Dynamics of Complex Technical Systems, Magdeburg,
Germany

²Institute of Experimental Internal Medicine, Magdeburg, Germany

³Process Systems Engineering Group, Otto von Guericke University, Magdeburg,
Germany

April 23, 2014

Contents

1	Data Processing	2
2	Modeling Approach	3
2.1	Dynamic Model structure	3
2.2	Modeling γ H2AX activation upon genotoxic stress	4
2.3	Model Equations	5
2.4	Parameter Inference	7
2.5	Profile Likelihood Analysis	11
3	Generated Data Sets	33

*flassig@mpi-magdeburg.mpg.de

1 Data Processing

The provided data constitute quantitative time-resolved immunoblotting data of γ H2AX (including replicates) and active p53 at different experimental conditions. The raw data were quantified with ImageJ (Schneider et al., 2012) to yield grey level intensities. The measured grey levels $y_{ij}(t)$ at time t can be related to the amount of antibodies $a_{ij}(t)$ (lumping first and secondary antibody effects) as

$$y_{ij}(t) = \beta_{0i} + \beta_{1i}a_{ij}(t), \quad (1)$$

where i represents the experimental run effects via β_{0i} background, and exposure β_{1i} . Index j represents experimental conditions (e.g. varying irradiation dose). The amount of antibodies can be related to the amount of proteins in a similar way as

$$a_{ij}(t) = \alpha_0 + \alpha_1p_{ij}(t), \quad (2)$$

whereas α_0 can be interpreted as unspecific binding effects and α_1 protein specific binding efficiency. The total protein amount in each lane $p_{ij}(t)$ is further affected by the loading i (loading effects, which belongs to experimental run effects) and the treatment j . In this form, lanes across one blot cannot be compared owing loading effects, let alone across different gels owing exposure, background, gel specific effects (e.g. transfer efficiency). Therefore, in order to allow (i) proper averaging over replicates as well as (ii) comparison amongst different experimental treatments, we have to normalize the quantified fluorescence levels. In the first step, different gels can be compared by normalizing the signals to a reference. Here we use the first time point of each signal. We then have

$$y_{ij}^+(t) = \frac{y_{ij}(t)}{y_{ij}(t=0)} = \frac{\alpha_0 + \alpha_1p_{ij}(t)}{\alpha_0 + \alpha_1p_{ij}(t=0)} \quad (3)$$

with removed backgrounds. The exposure term β_{1i} cancels out. Further, to account for loading effects we take the ratio

$$y_j^* = \frac{y_{ij}^+(t)}{c_i^+(t)} = \frac{\alpha_0 + \alpha_1p_{ij}(t)}{\xi_0 + \xi_1c_i(t)} \frac{\xi_0 + \xi_1c_i(t=0)}{\alpha_0 + \alpha_1p_{ij}(t=0)}, \quad (4)$$

where $c_i(t)$ represents the loading control / house keeping protein. The house keeping protein is not affected by different experimental conditions, i.e. index j is not present. In this way, we have reduced variations due to experimental parameter variations indexed with i , i.e. effects due to variations in between experimental runs. Equation (4) can be related to a simulated, average, relative protein amount $p_{j\text{sim}}(t)$ via

$$y_{j\text{sim}}^* = \frac{b_0 + b_1p_{j\text{sim}}(t)}{b_0 + b_1p_{j\text{sim}}(t=0)}, \quad (5)$$

where b_0 represents an offset and b_1 a scaling parameter.

Noise modeling: As has been shown by Kreutz et al. (2007) that experimental noise is best captured with a log-normal model. Therefore, data in the form of Eq. (4) as well as simulated response Eq. (5) are log-transformed. The final processed response data as well as the response model read

$$y_j = \log \left(\frac{y_j^+(t)}{c^+(t)} \right) \quad (6)$$

$$y_{j_{\text{sim}}} = \log \left(\frac{b_0 + b_1 p_{j_{\text{sim}}}(t)}{b_0 + b_1 p_{j_{\text{sim}}}(t=0)} \right). \quad (7)$$

Since we are modeling activation states of proteins upon stimulation, it is reasonable to assume $p_{j_{\text{sim}}}(t=0) = 0$ for activate states of each protein p under zero-stimulation condition. Then, Eq. 7 further simplifies to

$$y_{j_{\text{sim}}} = \log (1 + \text{scale}_p p_{j_{\text{sim}}}(t)), \quad (8)$$

with protein associated scaling parameter $\text{scale}_p = b_1/b_0$. This expression is used to relate measured signals of γ H2AX and p53-P in processed form, Eq. (6), to the simulated ones, Eq. (8).

Before parameter estimation, we performed a balanced two-way ANOVA (along immunoblot gels and time-points) on the processed data to identify replicates in the data sets that differed significantly from the others at a confidence level of 95%. These data sets were identified and removed from the data. In the case of γ H2AX the data variance was obtained from the sample variance. For p53-P, no replicates at the two different experimental conditions have been obtained. Therefore, the order of the variance of p53-P was estimated from the variance of the initial data.

2 Modeling Approach

2.1 Dynamic Model structure

The dynamics of the DNA damage response is modeled via ordinary differential equations. The dynamics of the internal states $\mathbf{x}(t, \mathbf{u}(t), \boldsymbol{\theta}_x) \in \mathbb{A}_x \subset \mathbb{R}^{n_x}$, represent relative protein concentrations (relative, since the data do not allow to set an absolute scale) and is determined by the solution of an initial value problem of the form

$$\frac{d}{dt} \mathbf{x}(t) = \mathbf{f}(\mathbf{x}(t), \mathbf{u}(t), \boldsymbol{\theta}_x) \quad (9)$$

with initial system states $\mathbf{x}(t_0) = \mathbf{x}_0$ and right hand side function $\mathbf{f}(\mathbf{x}(t), \mathbf{u}(t), \boldsymbol{\theta}_x)$ describing biologic interaction mechanisms, which depends on the system states $\mathbf{x}(t)$, (multiple) inputs $\mathbf{u}(t)$ (=stimulus), and kinetic parameter set $\boldsymbol{\theta}_x$. The readout variables are determined by

$$\mathbf{y}_{\text{sim}}(t, \boldsymbol{\theta}) = \mathbf{g}(\mathbf{x}(t, \boldsymbol{\theta}_x), \boldsymbol{\theta}_y), \quad (10)$$

where the function \mathbf{g} relates the internal system states to the readouts of the experiment with corresponding readout parameters $\boldsymbol{\theta}_y$, which together with dynamic parameters and initial conditions are merged into the model parameter vector $\boldsymbol{\theta} = [\boldsymbol{\theta}_x, \boldsymbol{\theta}_y]^T$, with redefined dynamic parameter vector $\boldsymbol{\theta}_x \equiv [\boldsymbol{\theta}_x, \mathbf{x}_0]^T$. The readout function is defined by Eq. (8).

2.2 Modeling γ H2AX activation upon genotoxic stress

Most of the interaction structure of the models has been constructed from available knowledge in the literature. The resulting topology is represented in Fig. 1. Ionizing radiation (IR) at a certain dose rate generates initial DSB (DDNA1) in a dose-dependent manner. Upon DSBs, cells trigger initial damage sensing and either use cNHEJ (fast) or HR/aNHEJ (slow) repair pathways. In detail, the damage signaling starts via the recognition of DDNA1 by Ku7080, its association to the damage site (RC11) and formation of the DNA-PK_{cs} complex (RC12). The catalytic subunit of DNA-PK_{cs} is then either phosphorylated by activated ATM or via autophosphorylation by DNA-PK_{cs} on the T2609 cluster, to initiate the NHEJ pathway (Chen et al., 2007). Here, we assume a two-step process as has been suggested by (Cucinotta et al., 2008). In parallel, the DSB can also be recognized by the MRN complex Mre11-Rad50-Nbs1, which can co-localize to the damage site to promote ATM activation, upon which ATM becomes autophosphorylated at Ser1981. This is modeled as a one step process as in (Mouri et al., 2009). One of the most important downstream targets of ATM during DDR is the tumor suppressor p53. Phosphorylation of p53 at Ser15 by ATM promotes its release from MDM2 and concomitantly its activation (Canman et al., 1998; Shieh et al., 1997). Activation of p53 by DNA-PK_{cs} has also been described in the literature (Lees-Miller et al., 1992). However, DNA-PK^{-/-} MEFs show normal p53 activation (Jimenez et al., 1999). We also did not find any evidence for a DNA-PK contribution, because the inhibition of DNA-PK_{cs} did not hamper the p53 phosphorylation (main document Fig. 2e). Therefore, we implemented the p53 activation as an ATM-dependent process only.

Failure to repair DSB via cNHEJ potentially releases DNA-PK_{cs} complexes and allows HR/aNHEJ repair proteins to access the damage site (Neal and Meek, 2011). These two major repair pathways split thus the initial DSB pool (DDNA1) into DDNA1 and DDNA2, whereas DDNA2 represents complex DSBs processed by HR/aNHEJ pathways. We model this branching from cNHEJ to HR/aNHEJ with a reaction triggered by active ATM. This is a reasonable assumption, since active ATM is required for HR/aNHEJ pathway activity (Koecher et al., 2012; Morrison et al., 2000). The detailed mechanisms that control the contribution of cNHEJ and HR/aNHEJ is not fully understood (Brandsma and Gent, 2012). We have generated four alternative models, which describe different mechanism of dynamic interaction of ATM, DNA-PK_{cs} and γ H2AX including the branching into cNHEJ and HR/aNHEJ repair pathways (see Fig. 1). Model complexity has been reduced to the necessary interaction steps in view of the modeling aim, i.e. investigating the contribution of ATM and DNA-PK_{cs} to γ H2AX activation on a dynamic basis. Proteins of large abundance in the cell have been assumed to be constant over the signaling time. In models A1 and A2, active ATM triggers the switch

to HR/aNHEJ before DDNA2, whereas in B1 and B2 the active ATM triggers after DDNA2. In A1 and B1 the active ATM as a trigger is modulated by the number of total DSBs, which is not the case in A2 and B2. These variants hypothesize, whether higher doses tend to induce more complex DSBs, which in turn need to be signaled to HR/aNHEJ. Since the initial signaling is restricted to the cell nucleus, the model describes the dynamics within the nucleus only.

From a pure signaling point of view, Ku7080 and MRN represent DSB signal sensors, whereas DNA-PK_{cs} and ATM (also ATR) DSB signal transducers. Similar to DNA-PK_{cs} in cNHEJ repair, Rad52 is a DSB repair mediator in HR. Repair by cNHEJ was modeled as a one-step process (RC12 to RDNA1). HR/aNHEJ have longer processing time, therefore a two-step process was assumed comprising association of Rad52 to DDNA2 and subsequent repair (RDNA2). Activation of γ H2AX is mediated by active DNA-PK_{cs} in single or double phosphorylated form or active ATM. Since the model is focusing on γ H2AX activation, which reflects the early phase in damage signaling, de-phosphorylation of γ H2AX is modeled as a simple first order reaction, independent of the repair process. The same holds for active ATM de-phosphorylation. All inactive forms of Ku7080, MRN, DNA-PK_{cs}, ATM, Rad52 and H2AX_{tot} are highly abundant. Their respective amounts in the cell are therefore assumed to be constant, which is especially valid when looking at the initial transient signaling. As a consequence, the hypothesized stabilization of ATM by DNA-PK_{cs} (in inactive form) is indirectly accounted for (Shrivastav et al., 2009). After OED I was performed, we added p53 to the models to better dissect individual contributions of DNA-PK_{cs} and ATM in combination with inhibitions experiments.

2.3 Model Equations

The model equations are scaled to the total concentration of $[\text{Ku7080}]_{\text{tot}}$ to make use of the intrinsic scale invariance of ODE in dimensional form to improve parameter estimation in terms of efficiency, see for instance supplement of Bachmann et al. (2011). Therefore, brackets - usually indicating a protein in concentration units - have been dropped, as the states of the ODE then represent relative concentration levels and are

thus dimensionless.

$$\text{initially damaged DNA:} \quad \frac{d}{dt} \text{DDNA1} = R_1 - R_2 \quad (11)$$

$$\text{complex \{Ku7080:DDNA1\}:} \quad \frac{d}{dt} \text{RC11} = R_2 - R_3 \quad (12)$$

$$\text{complex \{DNA-PK}_{cs}\text{:RC11\}:} \quad \frac{d}{dt} \text{RC12} = R_3 - R_4 - R_{6\mathcal{M}} \quad (13)$$

$$1^{st} \text{ phosphorylation step RC12:} \quad \frac{d}{dt} \text{RC12}^p = R_4 - R_5 \quad (14)$$

$$2^{nd} \text{ phosphorylation step RC12:} \quad \frac{d}{dt} \text{RC12}^{pp} = R_5 - R_7 \quad (15)$$

$$\text{complex damaged DNA:} \quad \frac{d}{dt} \text{DDNA2} = R_{6\mathcal{M}} - R_{9\mathcal{M}} \quad (16)$$

$$\text{complex \{MRN:DDNA1\}:} \quad \frac{d}{dt} \text{RC20} = R_{10} - R_{11} \quad (17)$$

$$\text{complex \{ATM:RC20\}:} \quad \frac{d}{dt} \text{RC21} = R_{11} - R_{12} \quad (18)$$

$$\text{double phosphorylated ATM:} \quad \frac{d}{dt} \text{RC21}^{pp} = R_{12} - R_{15} \quad (19)$$

$$\text{complex repair step:} \quad \frac{d}{dt} \text{RC22}^{pp} = R_{9\mathcal{M}} - R_8 \quad (20)$$

$$\text{repaired DNA:} \quad \frac{d}{dt} \text{RDNA1} = R_7 \quad (21)$$

$$\text{repaired DNA:} \quad \frac{d}{dt} \text{RDNA2} = R_8 \quad (22)$$

$$\gamma\text{H2AX:} \quad \frac{d}{dt} \gamma = R_{13} - R_{14} \quad (23)$$

$$\text{total damaged DNA:} \quad \frac{d}{dt} \text{tDSB} = R_1 \quad (24)$$

$$\text{phosphorylated p53:} \quad \frac{d}{dt} \text{p53}^p = R_{16} - R_{17} \quad (25)$$

Corresponding rates

$$R_1 = \alpha_0 \frac{dD}{dt} u(t) \quad (26)$$

$$R_2 = \alpha_{11} \text{DDNA1} \quad (27)$$

$$R_3 = \alpha_{12} \text{RC11} \quad (28)$$

$$R_4 = \alpha_{13} \text{RC12} \quad (29)$$

$$R_5 = \alpha_{141} (1 + \alpha_{142} \text{RC21}^{pp}) \text{RC12}^p \quad (30)$$

$$R_{6A1} = \alpha_{15} \text{tDSB RC21}^{pp} \text{RC12} \quad (31)$$

$$R_{6B1} = \alpha_{15} \text{tDSB RC12} \quad (32)$$

$$R_{6A2} = \alpha_{15} \text{RC21}^{pp} \text{RC12} \quad (33)$$

$$R_{6B2} = \alpha_{15} \text{RC12} \quad (34)$$

$$R_7 = \delta_{16} \text{RC12}^{pp} \quad (35)$$

$$R_8 = \delta_{16} \text{RC22}^{pp} \quad (36)$$

$$R_{9A12} = \alpha_{17} \text{DDNA2} \quad (37)$$

$$R_{9B12} = \alpha_{17} \text{RC21}^{pp} \text{DDNA2} \quad (38)$$

$$R_{10} = \alpha_{21} \text{DDNA1} \quad (39)$$

$$R_{11} = \alpha_{22} \text{RC20} \quad (40)$$

$$R_{12} = \alpha_{231} (1 + \alpha_{232} \text{RC21}^{pp}) \text{RC21} \quad (41)$$

$$R_{13} = \frac{a_{25} (\text{RC12}^p + \text{RC12}^{pp} + \text{RC21}^{pp})}{a_{25M} + \text{RC12}^p + \text{RC12}^{pp} + \text{RC21}^{pp}} (\xi - \gamma) \quad (42)$$

$$R_{14} = \alpha_{26} \gamma \quad (43)$$

$$R_{15} = \alpha_{23} \text{RC21}^{pp} \quad (44)$$

$$R_{16} = \alpha_{24} \text{RC21}^{pp} \quad (45)$$

$$R_{17} = \alpha_{25} \text{p53}^p. \quad (46)$$

Here, $u(t)$ represents the stimulus in form of a switching function, i.e. if the system is irradiated at dose rate $\frac{dD}{dt}$, $u(t) = 1$. If the system is not irradiated, $u(t) = 0$.

2.4 Parameter Inference

The parameters are estimated based on the maximum likelihood principle. Owing data processing, log-transform, noise model and ANOVA analysis (see Sec. 1), standard conditions can be assumed to hold. In fact, we verify this assumption after obtaining a fit by using Anderson-Darling statistics (see Tab. 1 in the main document). By this we also test model adequacy. We thus minimize the residual sum of squares

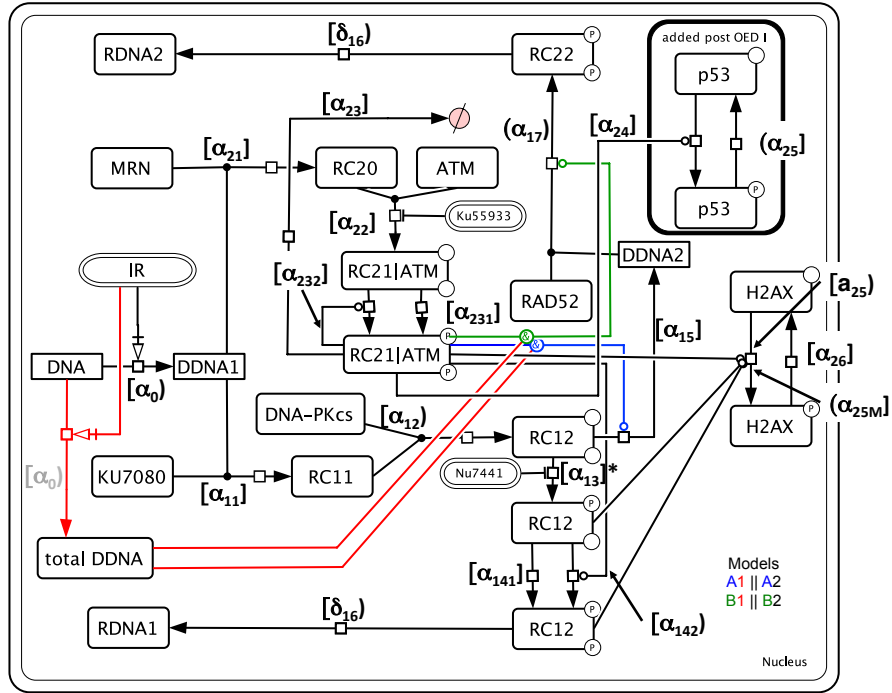
$$\chi^2(\boldsymbol{\theta}) = \sum_{i=1}^n \frac{(Y_i - y_{i\text{sim}}(\boldsymbol{\theta}))^2}{\sigma_Y^2} = \text{const.} - 2l(y_{i\text{sim}}(\boldsymbol{\theta})) \quad (47)$$

to yield a maximum likelihood estimate, where $l(y_{i_{\text{sim}}}(\boldsymbol{\theta}))$ represent the log-likelihood function, and summation is performed over all experimental data. Only the last term depends on $\boldsymbol{\theta}$. Therefore minimizing $\chi^2(\boldsymbol{\theta})$ with respect to $\boldsymbol{\theta}$ is equivalent to maximizing $l(\boldsymbol{\theta})$. The variance σ_Y^2 is estimated for each measured response and time point using the replicates in the data sets.

The objective function Eq. (47) itself was minimized using a hybrid optimization strategy, combining a genetic algorithm and interior-point/active-set optimization, which are implemented in MATLAB, to find a nearly global optimum. The models were also implemented in MATLAB and solved using the CVODES solver from (Hindmarsh et al., 2005). Rate constants and scaling parameters are positive and typically distributed on a logarithmic scale (Gutenkunst et al., 2007; Limpert et al., 2001). Therefore, the parameter estimation was performed on a logarithmic scale. Further, possible realizations of the kinetic parameters were constrained to the interval $[10^{-2} \dots 10^{+2}]$, whereas upper bounds of scaling parameters have been adjusted up to 10^4 . Overall, 19 kinetic parameters and 8 scaling parameters per model were estimated. As already mention above, initial conditions of the proteins where assumed to be zero, reflecting zero activity of the unperturbed states. The inactive proteins Ku7080, MRN, DNA-PK_{cs}, ATM and H2AX have large abundance, which allowed to reduce the number of parameters by assuming a constant supply of inactive to active protein forms. In the case of γ H2AX, the conservation relation

$$H2AX_{\text{tot}} = H2AX + \gamma H2AX \quad (48)$$

has been used to simplify the back reaction. The final parameter for the final identified model A2 are given in the Supplementary Table 1 in logarithmic representation. The lower and upper 95% point-wise confidence bounds are derived from the profile likelihood (see Sec. 2.5). Bounds with $\pm\infty$ indicate that the profile likelihood did not reach the critical value for significance. Notice that we have restricted the optimization effort for each model by constraining the parameter bounds on a range of 4 orders of magnitude in logarithmic space.



Supplementary Figure 1: The model structure is shown as an interaction graph, including 4 different versions of active ATM processing. Interactions are modeled via state transitions (arrows with squares), enzyme catalysis (lines with circles) and complex formation (joined lines). Stimulus and inhibitors have round-edge boxes. Activation of DNA-PK_{cs}, ATM and subsequent γ H2AX is modeled by two parallel pathways. The contribution to DNA DSB repair due to DNA-PK_{cs} or ATM signaling is modeled via branching of the damaged DNA pool resulting into a split of the initial damaged DSB DNA (DDNA1) into DDNA1 and DDNA2. Four mechanisms have been considered for branching (A1, A2, B1, B2). A and B refer to the location of the catalytic activity of ATM, which is used to model the availability of HR/aNHEJ proteins, as these depend on ATM activation. Index 1 and 2 refer to the kinetic law used. For models A/B in variant 1 branching to DDNA2 is catalyzed by the total amount of damaged DNA, which models the shift to HR/aNHEJ due to increased numbers of complex DSB at higher doses. Model variants A/B with index 2 do not use the total amount of damaged DNA. P53 has been added after OED I, as this was monitored during titration. Reaction parameters are also indicated, including the identifiability status (for model A2 only): parameter p is $[p]$ identifiable, $[p]^*$ identifiable, exceeding the upper optimization bound, $[p]$ non-identifiable upper limit, (p) non-identifiable lower limit, (p) structurally non-identifiable.

Supplementary Table 1: Final parameter set for model A2 and profile likelihood base lower and upper (LB,UB) 95% point-wise confidence bounds in log-space. Scaling parameters are represented as $\xi = \frac{[H2AX_{\text{tot}}]}{[\text{Ku7080}_{\text{tot}}]}$ and s_i and are in principle non-identifiable owing relative measurement data.

Parameter	Units	LB	$\log_{10}(\theta)$	UB
$\alpha_0 = \frac{a_0}{[\text{Ku7080}_{\text{tot}}]}$	Gy ⁻¹	1.2024	1.7262	∞
$\alpha_{11} = a_{11}[\text{Ku7080}_{\text{tot}}]$	min ⁻¹	-1.6041	-1.4588	-1.3195
$\alpha_{12} = a_{12}[\text{Ku7080}_{\text{tot}}]$	min ⁻¹	-0.2517	1.5123	∞
$\alpha_{13} = a_{13}[\text{Ku7080}_{\text{tot}}]$	min ⁻¹	1.8086	2.0000	∞
$\alpha_{141} = a_{141}[\text{Ku7080}_{\text{tot}}]$	min ⁻¹	-0.9869	-0.5246	-0.2279
$\alpha_{142} = \frac{a_{142}}{a_{141}}[\text{Ku7080}_{\text{tot}}]$	1	1.2977	1.7342	∞
$\alpha_{15} = a_{15}[\text{Ku7080}_{\text{tot}}]$	min ⁻¹	-0.7768	-0.2492	0.1913
$\delta_{16} = d_{16}[\text{Ku7080}_{\text{tot}}]$	1	1.4718	1.9601	∞
$\alpha_{17} = a_{17}[\text{Ku7080}_{\text{tot}}]$	min ⁻¹	$-\infty$	0.5089	∞
$\alpha_{21} = a_{21}[\text{Ku7080}_{\text{tot}}]$	min ⁻¹	-0.7612	-0.4635	0.2067
$\alpha_{22} = a_{22}[\text{Ku7080}_{\text{tot}}]$	min ⁻¹	-0.9253	-0.6773	-0.3882
$\alpha_{231} = a_{231}[\text{Ku7080}_{\text{tot}}]$	min ⁻¹	-1.7834	-0.3972	0.2888
$\alpha_{232} = a_{232}[\text{Ku7080}_{\text{tot}}]$	min ⁻¹	0.7257	1.2354	1.5524
a_{25}	min ⁻¹	0.2562	1.355	∞
$\alpha_{25M} = a_{25M}[\text{Ku7080}_{\text{tot}}]$	M ²	$-\infty$	-2	-1.8033
$\alpha_{26} = a_{26}[\text{Ku7080}_{\text{tot}}]$	min ⁻¹	-0.1947	0.6083	1.0618
$\alpha_{23} = a_{23}[\text{Ku7080}_{\text{tot}}]$	min ⁻¹	-0.0538	0.2526	1.1834
$\alpha_{24} = a_{24}[\text{Ku7080}_{\text{tot}}]$	min ⁻¹	-1.6565	-1.2240	-0.8093
$\alpha_{25} = a_{25}[\text{Ku7080}_{\text{tot}}]$	min ⁻¹	$-\infty$	-1.7197	-0.8152
$\xi = \frac{[H2AX_{\text{tot}}]}{[\text{Ku7080}_{\text{tot}}]}$	1	-	-0.6832	-
s_0	1	-	2.7705	-
s_1	1	-	2.4559	-
s_2	1	-	2.6787	-
s_3	1	-	2.7727	-
s_4	1	-	3.0366	-
s_5	1	-	1.9483	-
s_6	1	-	-1.0169	-

2.5 Profile Likelihood Analysis

For model A2, we calculated the profile likelihood χ_{PL}^2 as for instance described in (Raue et al., 2009), which we have implemented in MATLAB in combination with the fast CVODES ODE integration package (Hindmarsh et al., 2005). Absolute and relative tolerances have been set to 10^{-7} and 10^{-6} , respectively. The MATLAB implementation of the profile likelihood algorithm has been parallelized and is based on a template from the first author of (Raue et al., 2009). In Figures 2-20, we show the profile likelihoods for the kinetic parameters and the parameter dependencies in terms of relative parameter change for each kinetic parameter, when moving along the profile likelihood of each specific parameter in log-space. The relative parameter change of a parameter θ_m for increasing or decreasing parameter θ_n from its maximum likelihood estimate and $n \neq m$ is defined as

$$\delta\theta_{i,m} = \frac{\theta_{i,m} - \theta_m}{\theta_m}, \quad (49)$$

with index i representing a position along the profile likelihood of θ_n and θ_m being the maximum likelihood estimate of model A2, $m \in \{1, \dots, 19\} \setminus n$.

As a rough interpretation guide, flat profile likelihoods indicate non-identifiable parameters, whereas profile likelihood that pass the critical $\chi_{\alpha=0.05,df=1}^2$ value on both sides of the maximum-likelihood estimate of each parameter indicate an identifiable parameter. Profile likelihoods that hit the critical $\chi_{\alpha=0.05,df=1}^2$ value (in the Figures indicated by the red line) only on one side indicate practically non-identifiable parameters. In this case, at least the lower or upper bound of the parameter are bounded. Since we have only relative data, $\xi = \frac{[H2AX_{tot}]}{[Ku7080_{tot}]}$ and the readout scaling parameters are non-identifiable. This means, that the model cannot be used to predict absolute values of protein concentration. However, quantitative predictions regarding protein dynamics are possible. This is due to the fact, that the scaling parameters do not influence the right hand side of the ODE system. Like the authors of Bachmann et al. (2011), we thus treat scaling parameters as nuisance parameters.

Discussion on non-identifiable parameters:

Parameter α_0 has a non-identifiable upper bound for the given parameter estimation setup. The parameter represents the number of DNA double strand breaks per dose generated for a given dose rate. This means that the model structure has enough degrees of freedom to compensate higher but not too low DNA double strand breaks per dose rates for the given optimization setup. Thus, a minimal rate of DNA damage is needed to trigger the signaling. Compensation abilities by the model owing to limited information in the data is also apparent from the many parameter variations in terms of relative parameter change along the profile likelihood of α_0 . The parameter can be interpreted as a damage impact scaling parameter setting the scale of the downstream parameters. The qualitative behavior of protein dynamics is thus not changed.

α_{12} represents the complex formation step between Ku7080 and DNA-PK_{cs}. According to the profile likelihood bounds, a minimal rate of complex formation is needed, whereas the upper bound is unconstrained. This means that complex formation may be arbitrary fast, thus this reaction step may be neglected (model reduction). However, we leave this step in the model, as it represents a verified interaction (Chan et al., 2002; Cui et al., 2005; Ferguson et al., 2000; Martin et al., 2005).

If α_{13} is increased above the upper optimization constraint, it then becomes identifiable. This means, that in principle the parameter is identifiable.

α_{142} describes the catalysis of the second phosphorylation step of DNA-PK_{cs} by ATM and has an unconstrained upper bound. This means, that catalysis of ATM seems to be necessary, however several parameters can compensate increased catalytic activity of this reaction (see relative change of the parameters along the profile likelihood). For instance α_{141} , which represents the parallel reaction not catalyzed by ATM, anti-correlates with α_{142} . Note that α_{142} is identifiable owing to the data set where ATM is inhibited, which in turn makes the contribution of α_{142} negligible small and thus uncovers α_{141} .

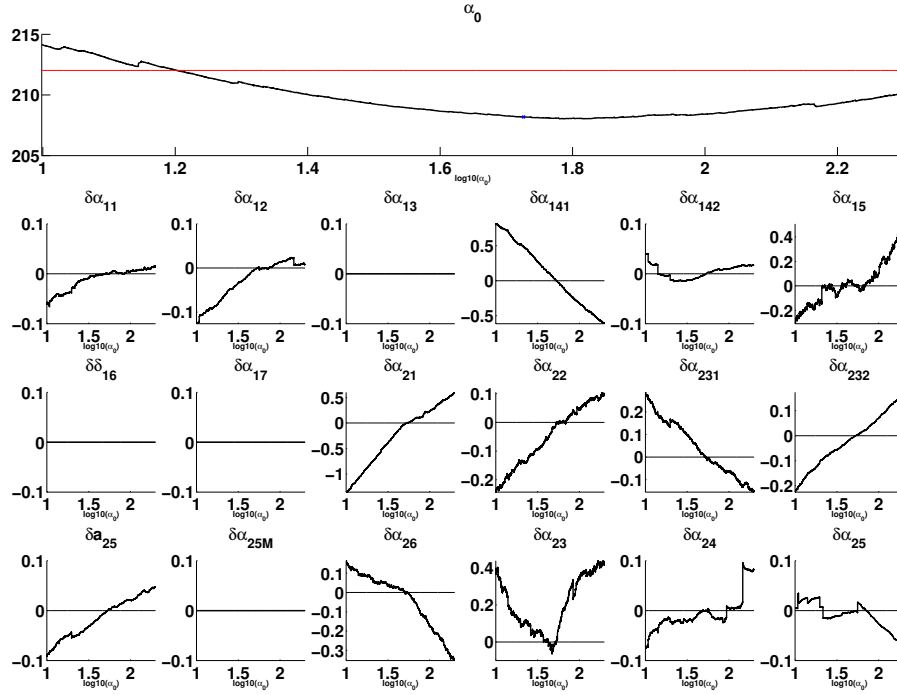
δ_{16} is used to model the final repair step for both, cNHEJ and HR/aNHEJ. This parameter has a lower bound, ensuring a minimal turnover of $RC21^{pp}$, which is related to the measurement signal. Since the upper bound of δ_{16} is unconstrained, both repair steps can be arbitrarily fast in the model.

Parameter α_{17} represents the reaction from Rad52 to RC22. As no measurement information is provided for this specific step, this reaction is thus unconstrained for the given data. Note that the subsequent δ_{16} reaction has a lower bound, since it is also used in the DNA-PK_{cs} part. In principle, this reaction can be withdrawn from the model to reduce model complexity.

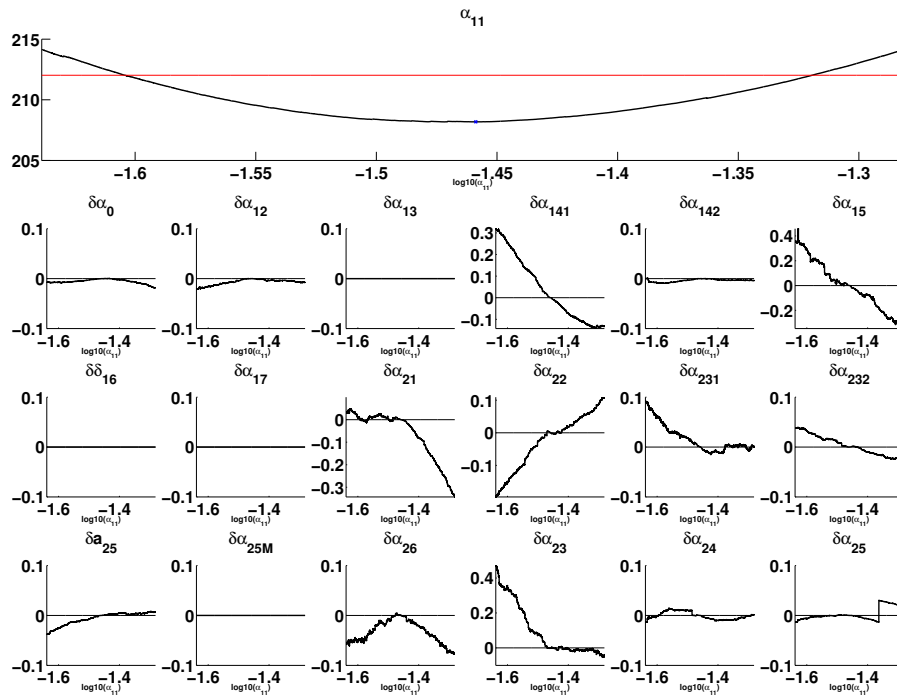
α_{25M} and a_{25} are both related to the activation of γ H2AX. Parameter a_{25} has an unconstrained upper bound, whereas α_{25M} is unconstrained on the lower bound. It can also be further reduced improving the overall fit.

Parameter α_{25} represents the degradation of p53-P and can in principle be arbitrarily fast.

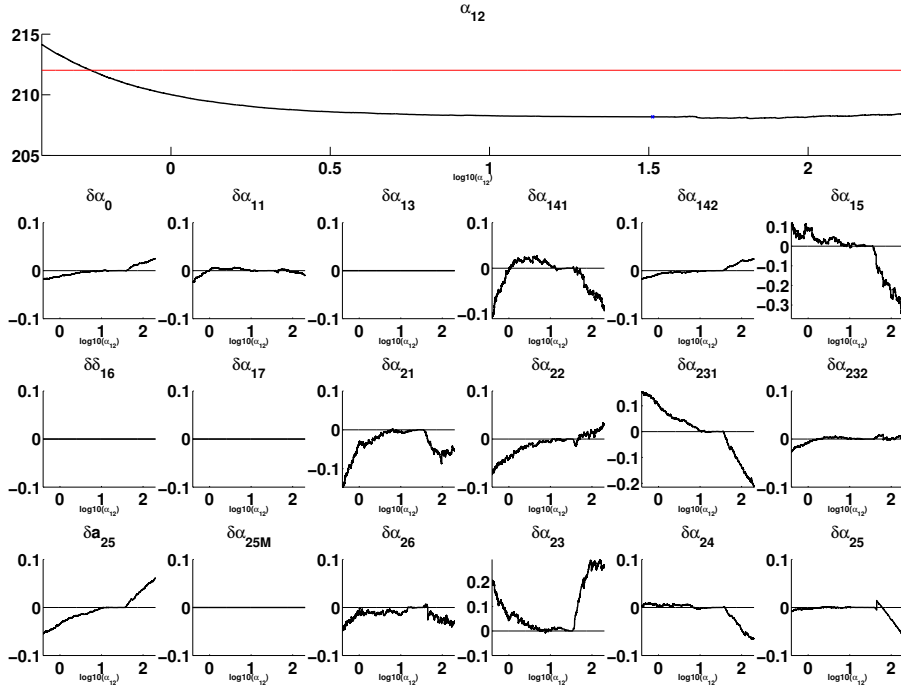
In Fig. 21 we show a simulation along the profile likelihood for all model states for a 5 Gy pulse. We see that the states associated to non-identifiable parameters have larger uncertainty bands. Even though γ H2AX has a noticeable uncertainty band, biphasic characteristics is however preserved and should still be observed experiments with suitable temporal resolution. Further, the small oscillatory part (visible in the panels of ATM-p (RC21^{pp}) of Fig. 21; Fig. 3 A in the main document) and γ H2AX signal) can be attributed to the feedback of ATM-p.



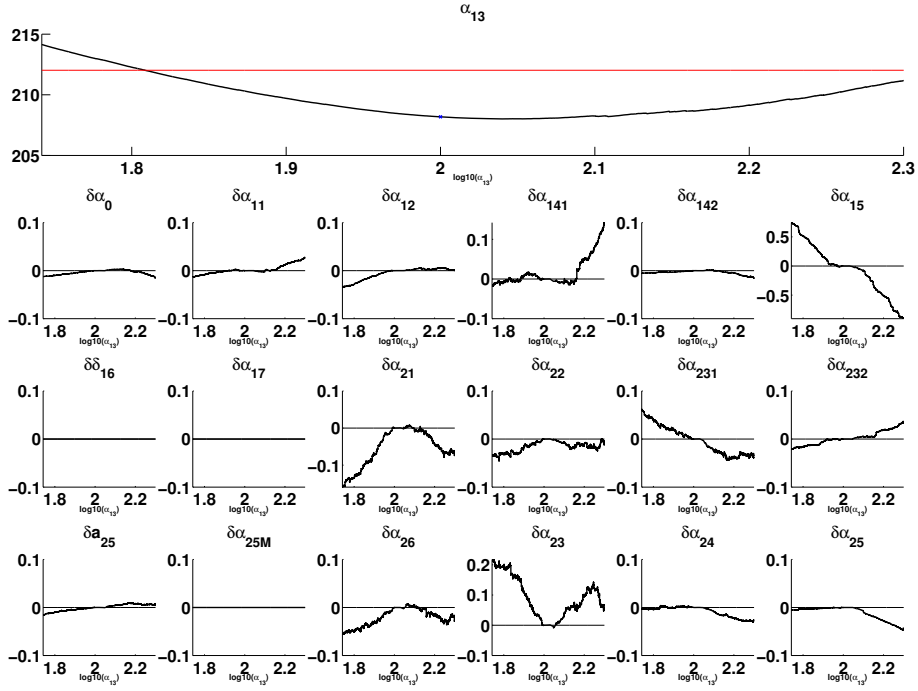
Supplementary Figure 2: Profile likelihood of model A2 for the specified kinetic parameter (upper panel, black line) and its dependencies on the remaining kinetic parameters in terms of relative change of each kinetic parameter in logspace (vertical axes of the small 3 x 6 subplots). The vertical axis in the upper panel indicates $\chi^2(\theta_i)$, which is proportional to -2 times the profile likelihood value, whereas the horizontal axis represents the parameter value in logspace. The red line in the upper panel indicates the critical value for significance. The parameter value of the point estimate is indicated by a small blue cross in the upper panel.



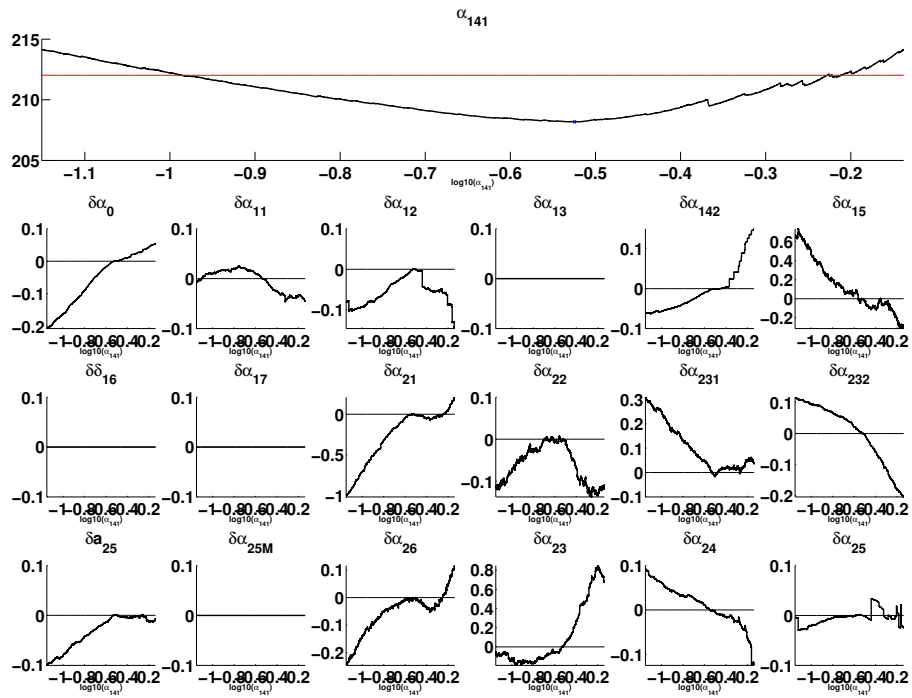
Supplementary Figure 3: Profile likelihood of model A2 for the specified kinetic parameter (upper panel, black line) and its dependencies on the remaining kinetic parameters in terms of relative change of each kinetic parameter in logspace (vertical axes of the small 3 x 6 subplots). The vertical axis in the upper panel indicates $\chi^2(\theta_i)$, which is proportional to -2 times the profile likelihood value, whereas the horizontal axis represents the parameter value in logspace. The red line in the upper panel indicates the critical value for significance. The parameter value of the point estimate is indicated by a small blue cross in the upper panel.



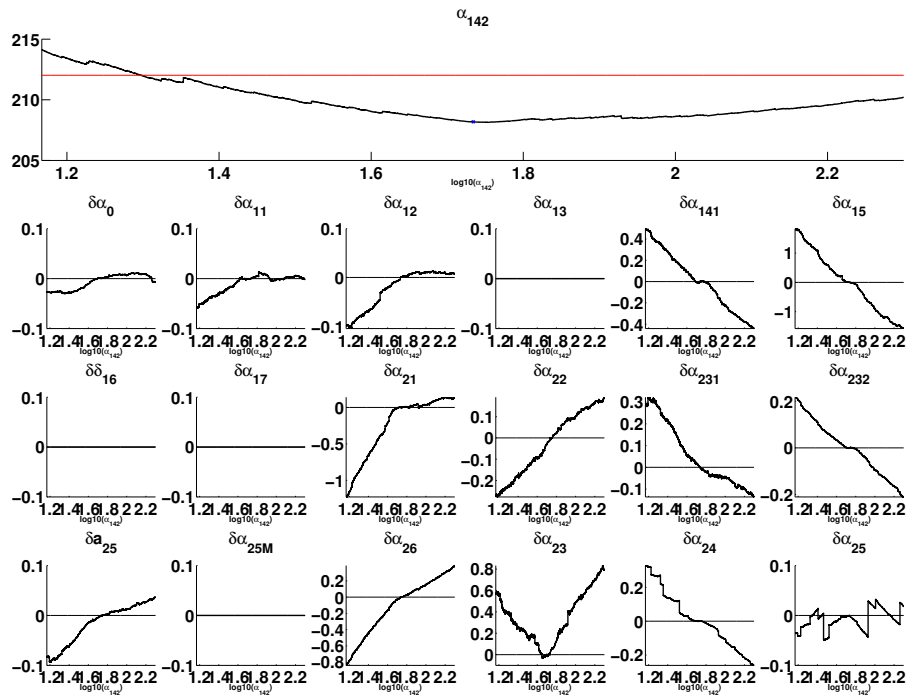
Supplementary Figure 4: Profile likelihood of model A2 for the specified kinetic parameter (upper panel, black line) and its dependencies on the remaining kinetic parameters in terms of relative change of each kinetic parameter in logspace (vertical axes of the small 3 x 6 subplots). The vertical axis in the upper panel indicates $\chi^2(\theta_i)$, which is proportional to -2 times the profile likelihood value, whereas the horizontal axis represents the parameter value in logspace. The red line in the upper panel indicates the critical value for significance. The parameter value of the point estimate is indicated by a small blue cross in the upper panel.



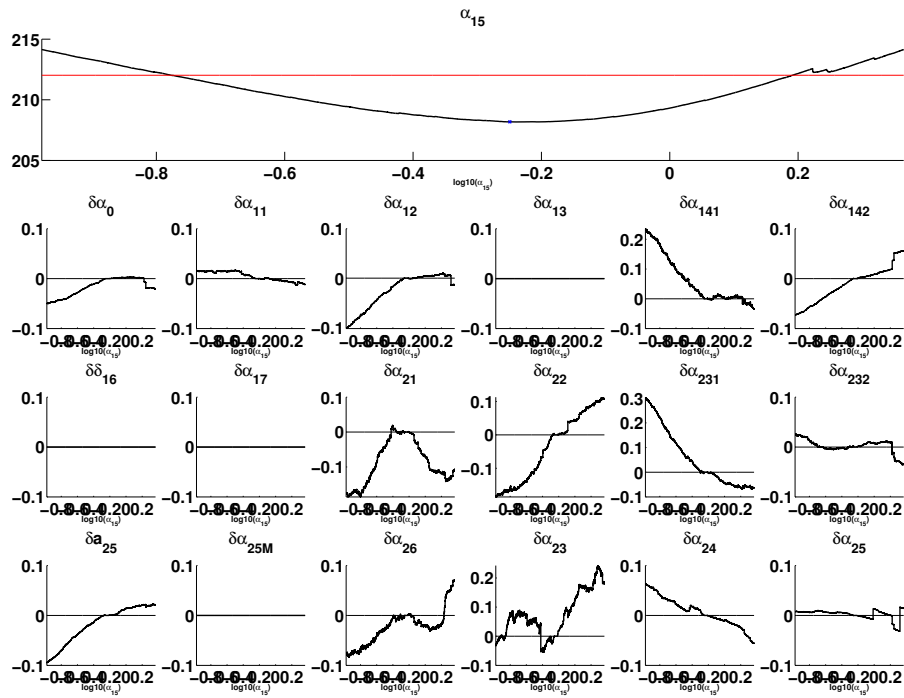
Supplementary Figure 5: Profile likelihood of model A2 for the specified kinetic parameter (upper panel, black line) and its dependencies on the remaining kinetic parameters in terms of relative change of each kinetic parameter in logspace (vertical axes of the small 3 x 6 subplots). The vertical axis in the upper panel indicates $\chi^2(\theta_i)$, which is proportional to -2 times the profile likelihood value, whereas the horizontal axis represents the parameter value in logspace. The red line in the upper panel indicates the critical value for significance. The parameter value of the point estimate is indicated by a small blue cross in the upper panel.



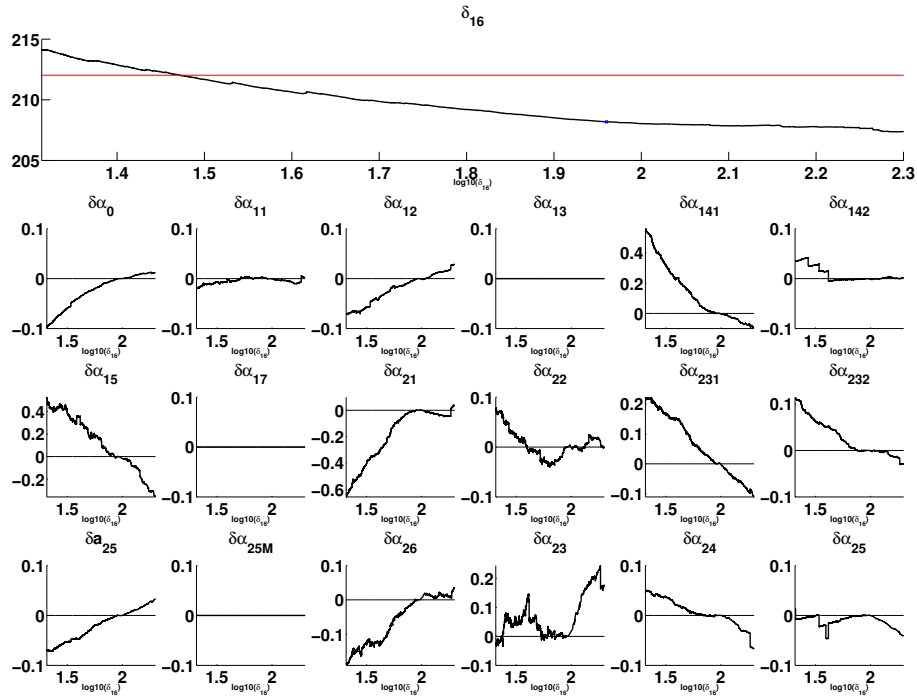
Supplementary Figure 6: Profile likelihood of model A2 for the specified kinetic parameter (upper panel, black line) and its dependencies on the remaining kinetic parameters in terms of relative change of each kinetic parameter in logspace (vertical axes of the small 3 x 6 subplots). The vertical axis in the upper panel indicates $\chi^2(\theta_i)$, which is proportional to -2 times the profile likelihood value, whereas the horizontal axis represents the parameter value in logspace. The red line in the upper panel indicates the critical value for significance. The parameter value of the point estimate is indicated by a small blue cross in the upper panel.



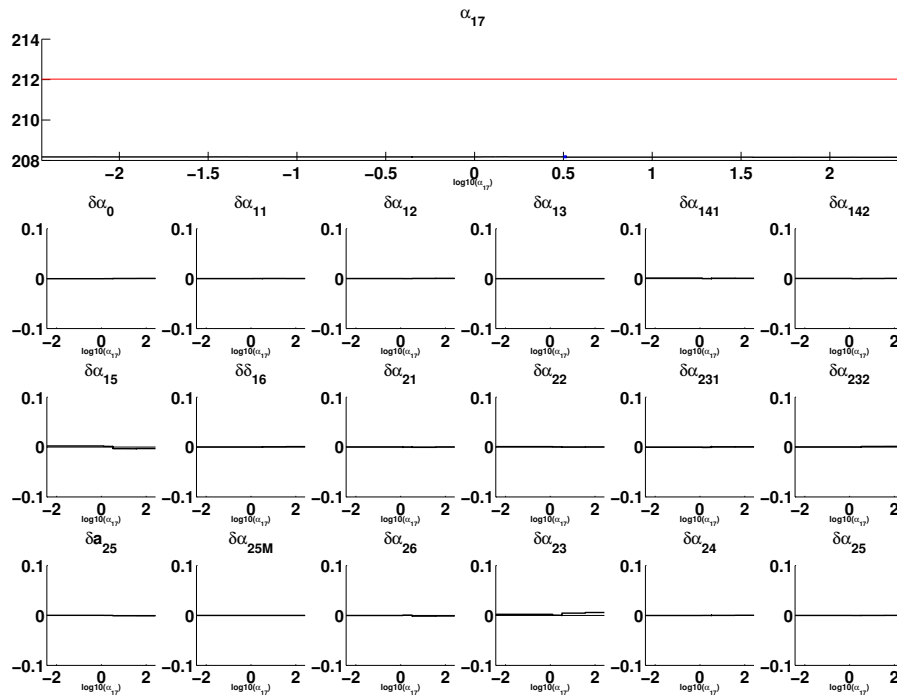
Supplementary Figure 7: Profile likelihood of model A2 for the specified kinetic parameter (upper panel, black line) and its dependencies on the remaining kinetic parameters in terms of relative change of each kinetic parameter in logspace (vertical axes of the small 3 x 6 subplots). The vertical axis in the upper panel indicates $\chi^2(\theta_i)$, which is proportional to -2 times the profile likelihood value, whereas the horizontal axis represents the parameter value in logspace. The red line in the upper panel indicates the critical value for significance. The parameter value of the point estimate is indicated by a small blue cross in the upper panel.



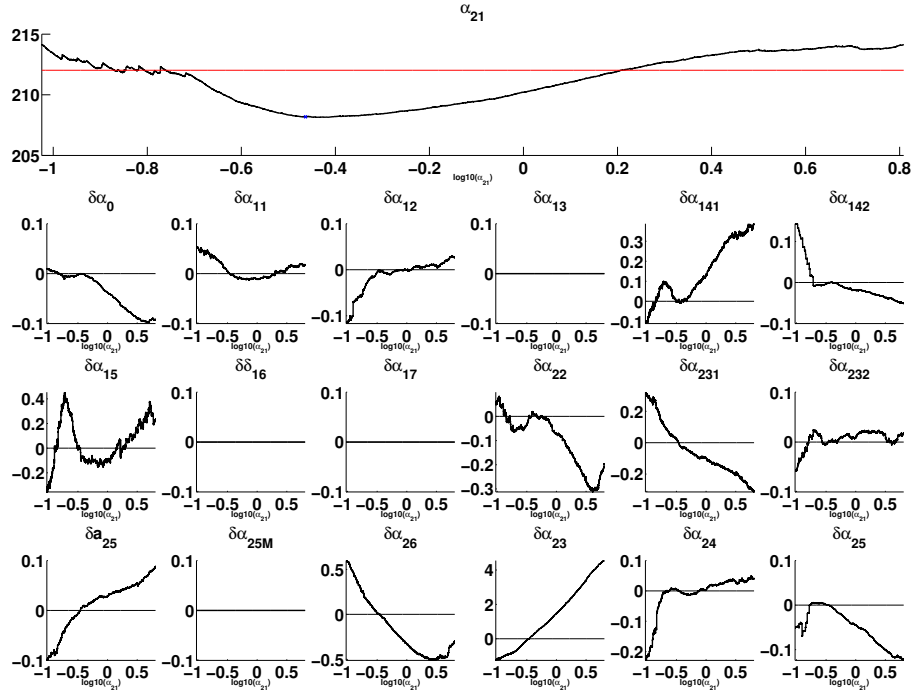
Supplementary Figure 8: Profile likelihood of model A2 for the specified kinetic parameter (upper panel, black line) and its dependencies on the remaining kinetic parameters in terms of relative change of each kinetic parameter in logspace (vertical axes of the small 3 x 6 subplots). The vertical axis in the upper panel indicates $\chi^2(\theta_i)$, which is proportional to -2 times the profile likelihood value, whereas the horizontal axis represents the parameter value in logspace. The red line in the upper panel indicates the critical value for significance. The parameter value of the point estimate is indicated by a small blue cross in the upper panel.



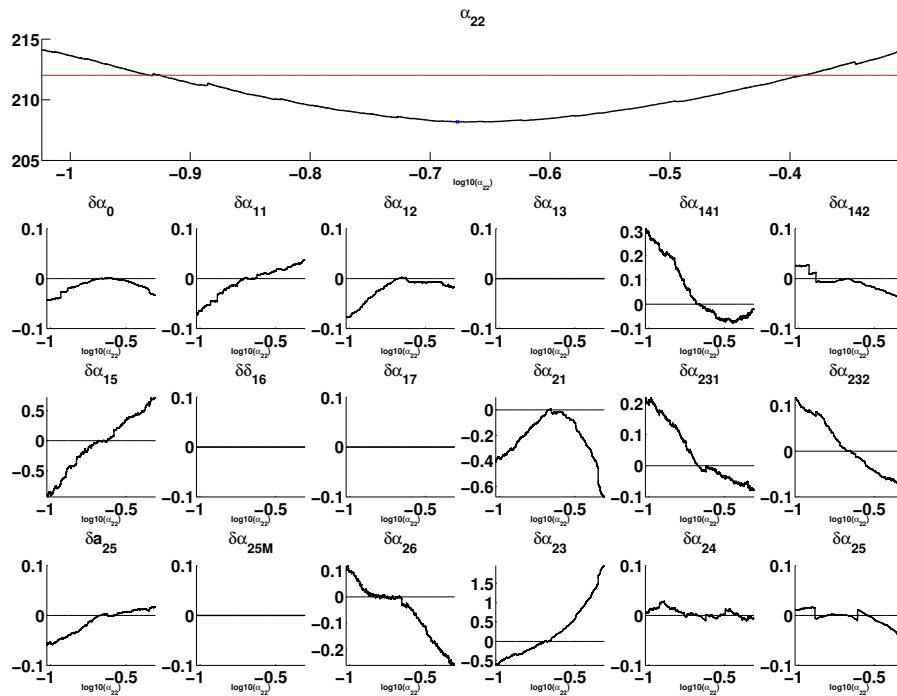
Supplementary Figure 9: Profile likelihood of model A2 for the specified kinetic parameter (upper panel, black line) and its dependencies on the remaining kinetic parameters in terms of relative change of each kinetic parameter in logspace (vertical axes of the small 3 x 6 subplots). The vertical axis in the upper panel indicates $\chi^2(\theta_i)$, which is proportional to -2 times the profile likelihood value, whereas the horizontal axis represents the parameter value in logspace. The red line in the upper panel indicates the critical value for significance. The parameter value of the point estimate is indicated by a small blue cross in the upper panel.



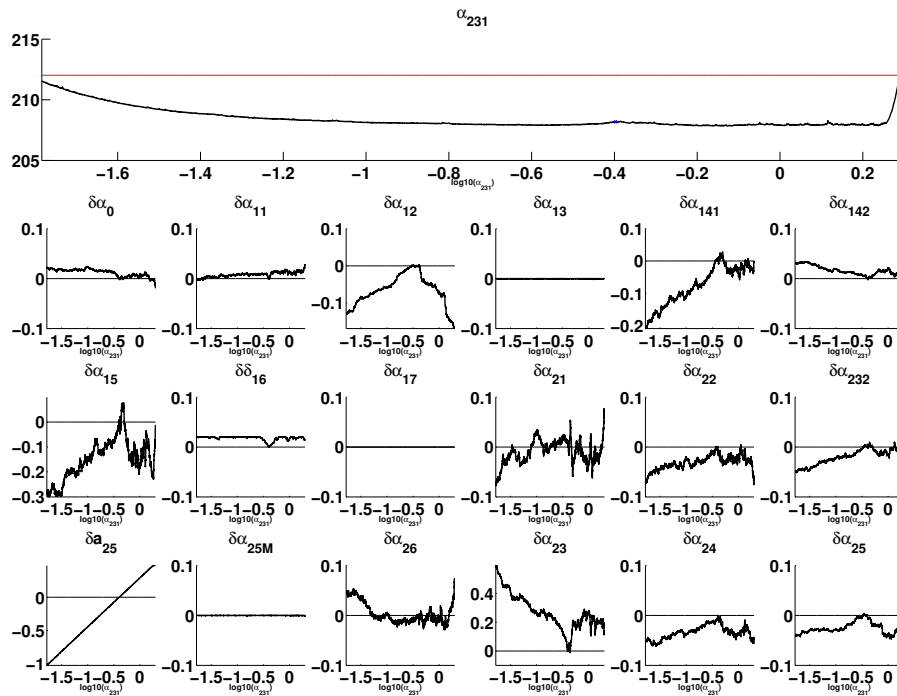
Supplementary Figure 10: Profile likelihood of model A2 for the specified kinetic parameter (upper panel, black line) and its dependencies on the remaining kinetic parameters in terms of relative change of each kinetic parameter in logspace (vertical axes of the small 3 x 6 subplots). The vertical axis in the upper panel indicates $\chi^2(\theta_i)$, which is proportional to -2 times the profile likelihood value, whereas the horizontal axis represents the parameter value in logspace. The red line in the upper panel indicates the critical value for significance. The parameter value of the point estimate is indicated by a small blue cross in the upper panel.



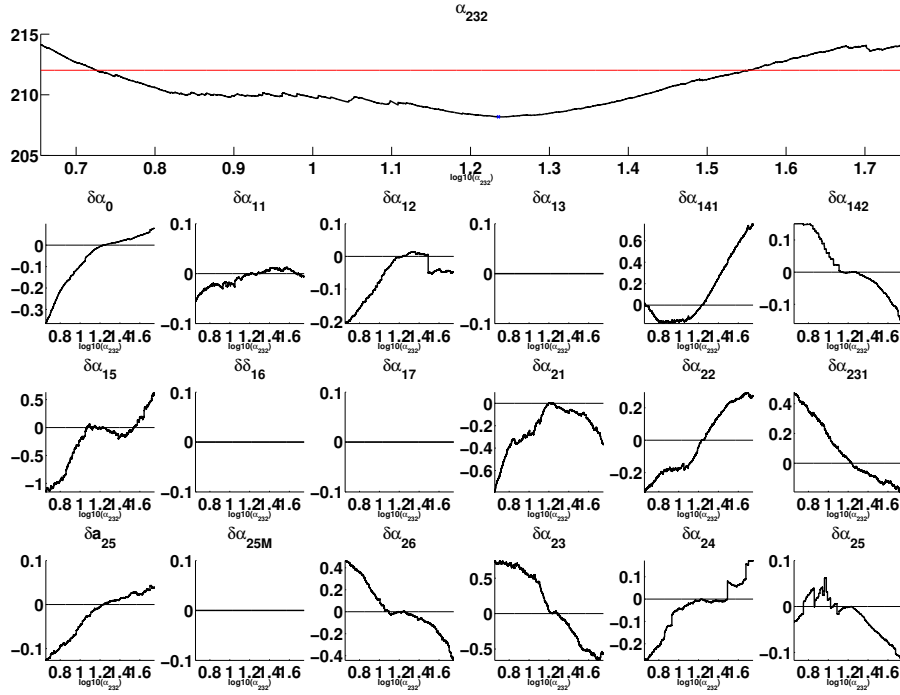
Supplementary Figure 11: Profile likelihood of model A2 for the specified kinetic parameter (upper panel, black line) and its dependencies on the remaining kinetic parameters in terms of relative change of each kinetic parameter in logspace (vertical axes of the small 3 x 6 subplots). The vertical axis in the upper panel indicates $\chi^2(\theta_i)$, which is proportional to -2 times the profile likelihood value, whereas the horizontal axis represents the parameter value in logspace. The red line in the upper panel indicates the critical value for significance. The parameter value of the point estimate is indicated by a small blue cross in the upper panel.



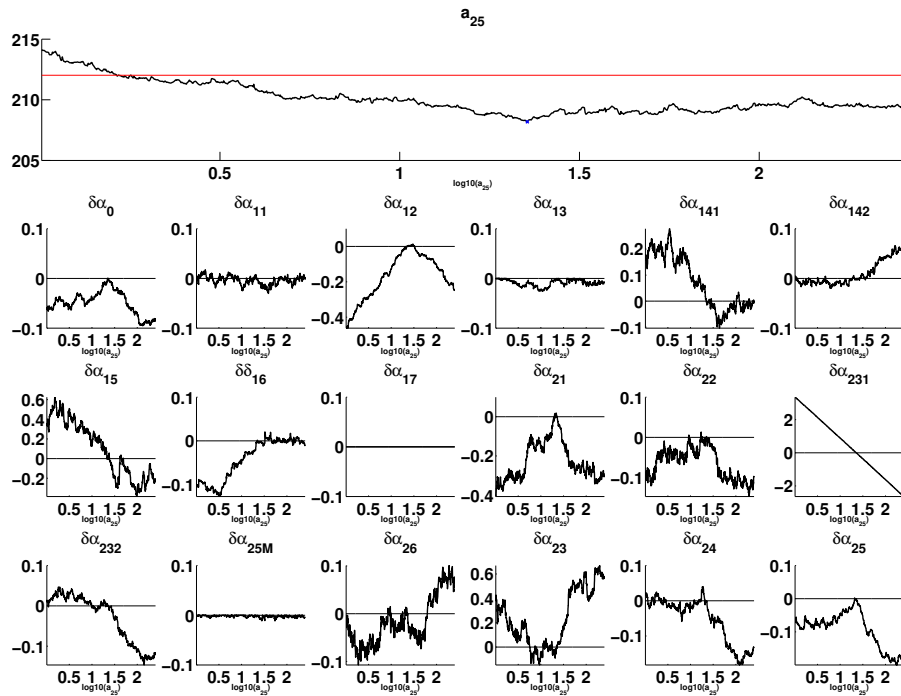
Supplementary Figure 12: Profile likelihood of model A2 for the specified kinetic parameter (upper panel, black line) and its dependencies on the remaining kinetic parameters in terms of relative change of each kinetic parameter in logspace (vertical axes of the small 3 x 6 subplots). The vertical axis in the upper panel indicates $\chi^2(\theta_i)$, which is proportional to -2 times the profile likelihood value, whereas the horizontal axis represents the parameter value in logspace. The red line in the upper panel indicates the critical value for significance. The parameter value of the point estimate is indicated by a small blue cross in the upper panel.



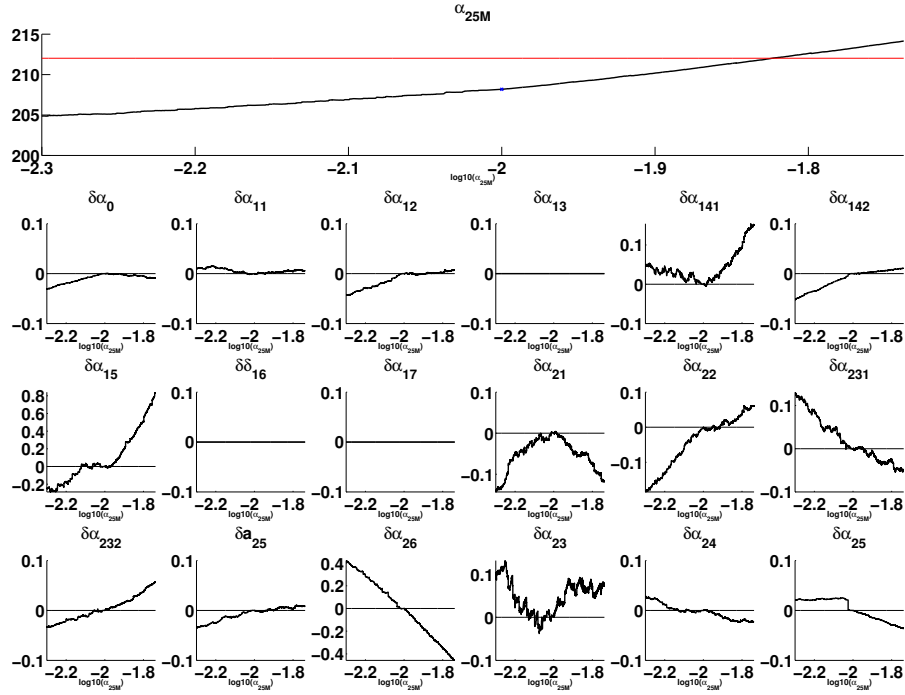
Supplementary Figure 13: Profile likelihood of model A2 for the specified kinetic parameter (upper panel, black line) and its dependencies on the remaining kinetic parameters in terms of relative change of each kinetic parameter in logspace (vertical axes of the small 3 x 6 subplots). The vertical axis in the upper panel indicates $\chi^2(\theta_i)$, which is proportional to -2 times the profile likelihood value, whereas the horizontal axis represents the parameter value in logspace. The red line in the upper panel indicates the critical value for significance. The parameter value of the point estimate is indicated by a small blue cross in the upper panel.



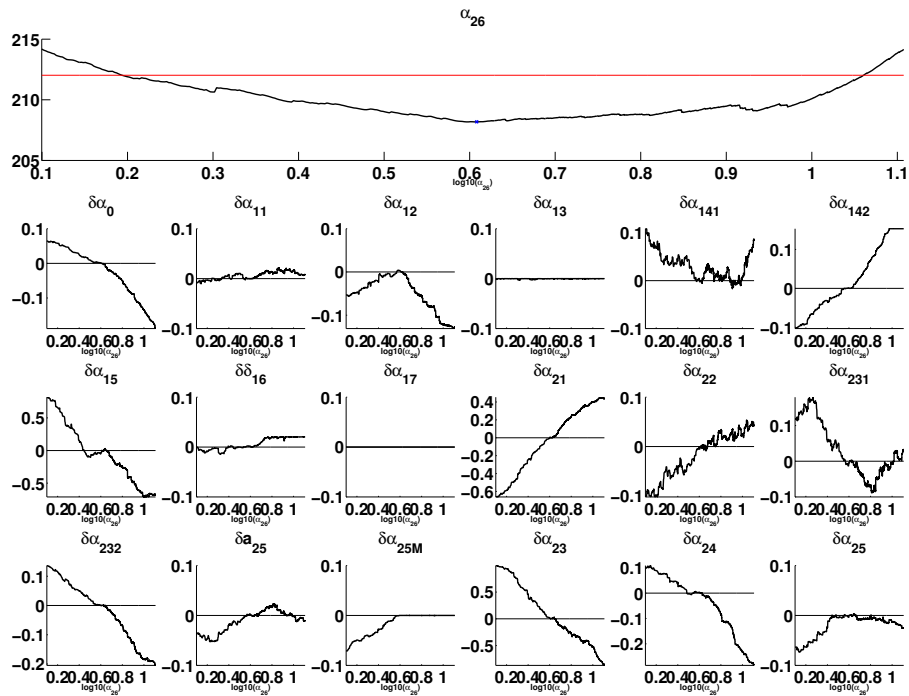
Supplementary Figure 14: Profile likelihood of model A2 for the specified kinetic parameter (upper panel, black line) and its dependencies on the remaining kinetic parameters in terms of relative change of each kinetic parameter in logspace (vertical axes of the small 3 x 6 subplots). The vertical axis in the upper panel indicates $\chi^2(\theta_i)$, which is proportional to -2 times the profile likelihood value, whereas the horizontal axis represents the parameter value in logspace. The red line in the upper panel indicates the critical value for significance. The parameter value of the point estimate is indicated by a small blue cross in the upper panel.



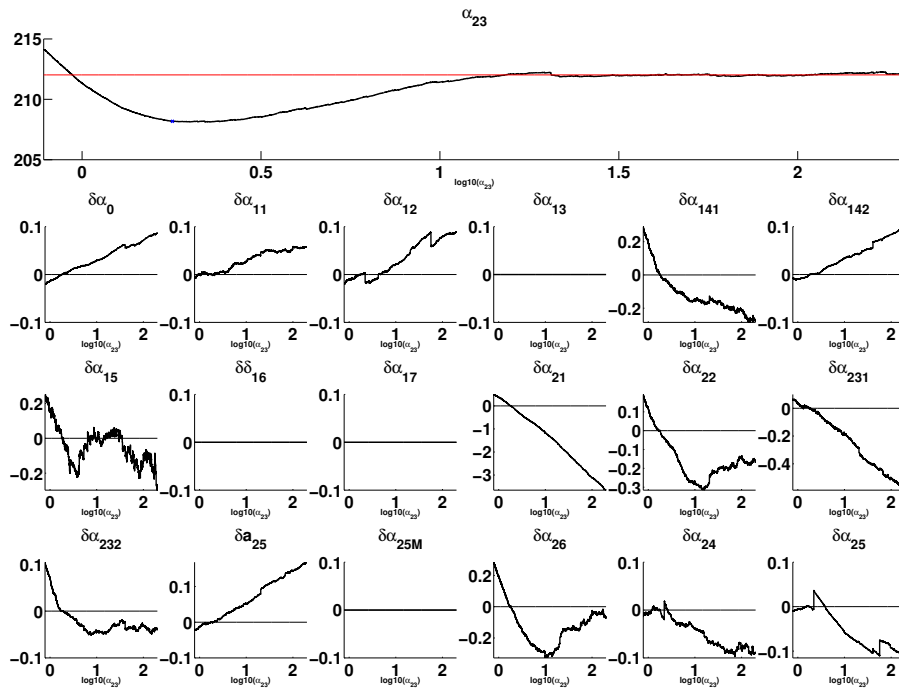
Supplementary Figure 15: Profile likelihood of model A2 for the specified kinetic parameter (upper panel, black line) and its dependencies on the remaining kinetic parameters in terms of relative change of each kinetic parameter in logspace (vertical axes of the small 3 x 6 subplots). The vertical axis in the upper panel indicates $\chi^2(\theta_i)$, which is proportional to -2 times the profile likelihood value, whereas the horizontal axis represents the parameter value in logspace. The red line in the upper panel indicates the critical value for significance. The parameter value of the point estimate is indicated by a small blue cross in the upper panel.



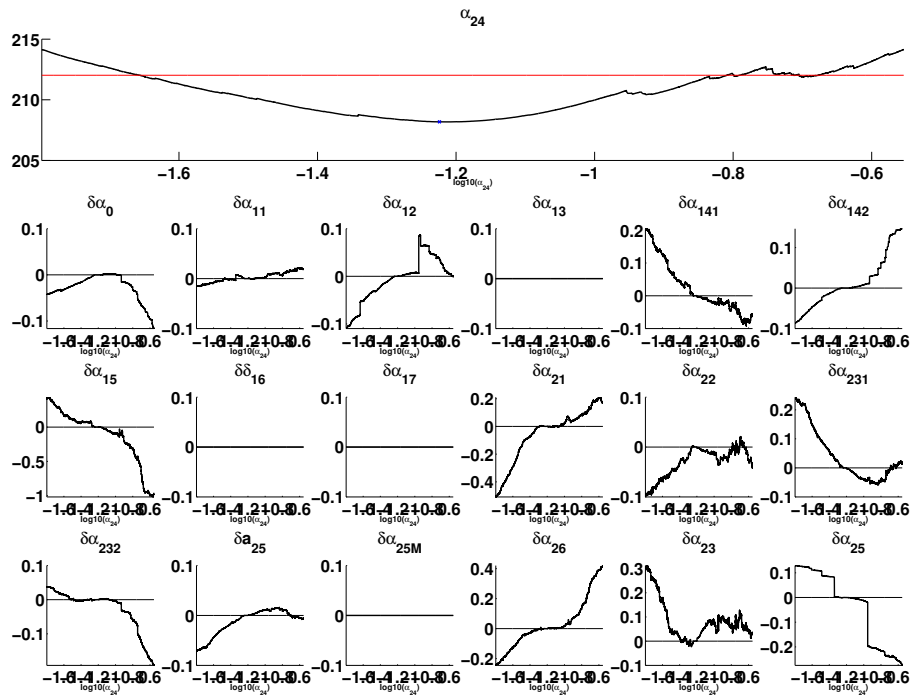
Supplementary Figure 16: Profile likelihood of model A2 for the specified kinetic parameter (upper panel, black line) and its dependencies on the remaining kinetic parameters in terms of relative change of each kinetic parameter in logspace (vertical axes of the small 3 x 6 subplots). The vertical axis in the upper panel indicates $\chi^2(\theta_i)$, which is proportional to -2 times the profile likelihood value, whereas the horizontal axis represents the parameter value in logspace. The red line in the upper panel indicates the critical value for significance. The parameter value of the point estimate is indicated by a small blue cross in the upper panel.



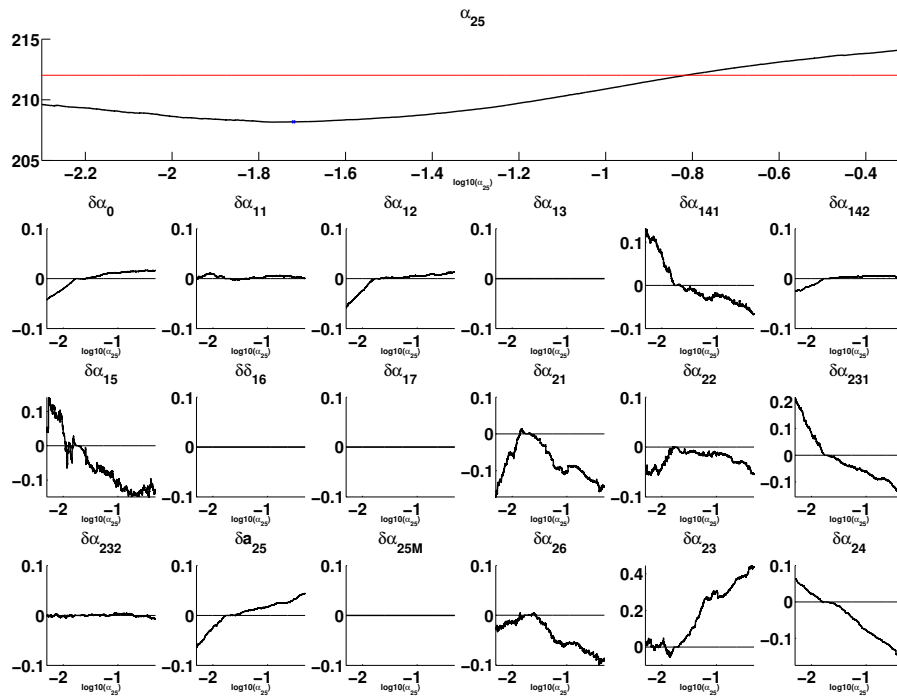
Supplementary Figure 17: Profile likelihood of model A2 for the specified kinetic parameter (upper panel, black line) and its dependencies on the remaining kinetic parameters in terms of relative change of each kinetic parameter in logspace (vertical axes of the small 3 x 6 subplots). The vertical axis in the upper panel indicates $\chi^2(\theta_i)$, which is proportional to -2 times the profile likelihood value, whereas the horizontal axis represents the parameter value in logspace. The red line in the upper panel indicates the critical value for significance. The parameter value of the point estimate is indicated by a small blue cross in the upper panel.



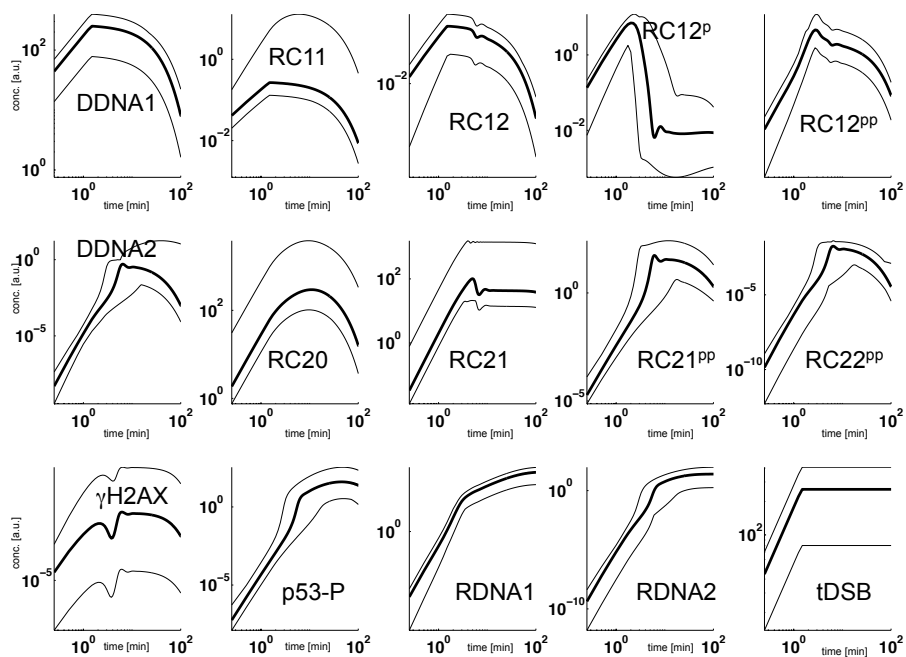
Supplementary Figure 18: Profile likelihood of model A2 for the specified kinetic parameter (upper panel, black line) and its dependencies on the remaining kinetic parameters in terms of relative change of each kinetic parameter in logspace (vertical axes of the small 3 x 6 subplots). The vertical axis in the upper panel indicates $\chi^2(\theta_i)$, which is proportional to -2 times the profile likelihood value, whereas the horizontal axis represents the parameter value in logspace. The red line in the upper panel indicates the critical value for significance. The parameter value of the point estimate is indicated by a small blue cross in the upper panel.



Supplementary Figure 19: Profile likelihood of model A2 for the specified kinetic parameter (upper panel, black line) and its dependencies on the remaining kinetic parameters in terms of relative change of each kinetic parameter in logspace (vertical axes of the small 3 x 6 subplots). The vertical axis in the upper panel indicates $\chi^2(\theta_i)$, which is proportional to -2 times the profile likelihood value, whereas the horizontal axis represents the parameter value in logspace. The red line in the upper panel indicates the critical value for significance. The parameter value of the point estimate is indicated by a small blue cross in the upper panel.



Supplementary Figure 20: Profile likelihood of model A2 for the specified kinetic parameter (upper panel, black line) and its dependencies on the remaining kinetic parameters in terms of relative change of each kinetic parameter in logspace (vertical axes of the small 3 x 6 subplots). The vertical axis in the upper panel indicates $\chi^2(\theta_i)$, which is proportional to -2 times the profile likelihood value, whereas the horizontal axis represents the parameter value in logspace. The red line in the upper panel indicates the critical value for significance. The parameter value of the point estimate is indicated by a small blue cross in the upper panel.



Supplementary Figure 21: Model states for a 5 Gy pulse and confidence bands (thin black lines) derived from the profile likelihood. For illustration purpose axes are on log-scale. The time window is from 0 to 100 minutes.

3 Generated Data Sets

Initial Data Set The initial data set represents time course data of γ H2AX for 0.5, 1, 2, 5 and 40 Gy at a dose rate of 3.332 Gy/min including repetitions.

Supplementary Table 2: Part of the initial, processed data set including repetitions for γ H2AX in arbitrary units at 0.5 Gy.

time [min]	replicate 1	replicate 2	replicate 3	mean	variance
0	0	0	0	0	0
30.0000	0.3392	0.5438	0.3223	0.4018	0.0152
90.0000	0.1149	0.4700	0.0561	0.2137	0.0502
180.0000	-0.0254	0.2590	-0.0634	0.0568	0.0310
300.0000	-0.0546	0.3194	-0.1082	0.0522	0.0543
720.0000	-0.3309	0.3717	-0.0962	-0.0185	0.1280

Supplementary Table 3: Part of the initial, processed data set including repetitions for γ H2AX in arbitrary units at 1 Gy.

time [min]	replicate 1	replicate 2	replicate 3	mean	variance
0	0	0	0	0	0
30.0000	0.3416	0.1623	0.5049	0.3362	0.0294
90.0000	0.0844	-0.1095	0.0161	-0.0030	0.0097
180.0000	0.0231	-0.2766	-0.0151	-0.0895	0.0266
300.0000	0.1444	-0.3489	0.1186	-0.0286	0.0771
720.0000	0.1014	-0.8443	-0.2728	-0.3386	0.2268

Data Set for Optimal Design D_1^* The data set represents time course data of γ H2AX for the optimized double pulse of 1 Gy at time $t = 0$ min and 20 Gy at time $t = 360$ min, both at a dose rates of 3.332 Gy/min including repetitions.

Supplementary Table 4: Part of the initial, processed data set including repetitions for γ H2AX in arbitrary units at 2 Gy.

time [min]	rep. 1	rep. 2	rep. 3	rep. 4	rep. 5	mean	variance
0	0	0	0	0	0	0	0
30.0000	0.5681	0.9821	0.6178	0.3252	0.3657	0.5718	0.0684
90.0000	0.2436	0.6653	0.2415	0.0667	0.0634	0.2561	0.0602
180.0000	-0.0406	0.3705	0.0789	-0.0966	0.0236	0.0671	0.0331
300.0000	-0.0654	0.3057	0.1438	-0.2495	-0.2712	-0.0273	0.0626
720.0000	0.1207	0.4834	0.3147	-0.2747	-0.2334	0.0821	0.1109

Supplementary Table 5: Part of the initial, processed data set including repetitions for γ H2AX in arbitrary units at 5 Gy.

time [min]	rep. 1	rep. 2	rep. 3	rep. 4	mean	variance
0	0	0	0	0	0	0
30.0000	0.3191	0.4677	0.2570	0.8668	0.4776	0.0751
90.0000	0.1627	0.0688	0.0179	0.4109	0.1651	0.0305
180.0000	-0.1855	-0.1512	-0.2190	0.3148	-0.0602	0.0633
300.0000	-0.0500	0.0001	-0.1764	-0.0034	-0.0574	0.0068
720.0000	-0.0641	-0.0230	-0.1582	0.7630	0.1294	0.1816

Supplementary Table 6: Part of the initial, processed data set including repetitions for γ H2AX in arbitrary units at 40 Gy.

time [min]	rep. 1	rep. 2	rep. 3	rep. 4	mean	variance
0	0	0	0	0	0	0
30.0000	1.6426	1.0232	0.6457	0.8407	1.0381	0.1862
90.0000	1.7743	0.8925	0.6072	0.6837	0.9894	0.2883
180.0000	1.3355	0.6076	0.6076	0.2323	0.6957	0.2132
300.0000	1.1927	0.3388	0.4196	0.0833	0.5086	0.2286
720.0000	0.7881	-0.0271	0.2081	-0.1396	0.2074	0.1709

Supplementary Table 7: Processed data set including repetitions for γ H2AX in arbitrary units for the optimized design \mathbf{D}_1^* .

time [min]	replicate 1	replicate 2	replicate 3	mean	variance
0	0	0	0	0	0
15.0000	0.2722	0.3709	0.1474	0.2635	0.0125
35.0000	0.1215	0.3145	0.1057	0.1806	0.0135
60.0000	-0.0805	0.3183	0.1245	0.1208	0.0398
160.0000	-0.2712	0.2290	0.0214	-0.0069	0.0632
240.0000	-0.1223	0.2553	-0.0195	0.0378	0.0381
370.0000	0.8405	0.7530	0.6690	0.7542	0.0074
420.0000	0.8336	0.6858	0.5358	0.6851	0.0222
450.0000	0.4571	0.6582	0.4958	0.5370	0.0114

Data Set p53-P from titration experiments P53-P data obtained for a double pulse of 1 Gy at time $t = 0$ min and 20 Gy at time $t = 360$ min.

Supplementary Table 8: Part of the initial, processed data set without repetitions for p53-P in arbitrary units for a double pulse of 1Gy and 20 Gy at time $t = 360$ min and application of $1\mu\text{M}$ Ku55933.

time [min]	rep. 1
0	0
35.0000	0.0253
370.0000	0.7520

Supplementary Table 9: Part of the initial, processed data set without repetitions for p53-P in arbitrary units for a double pulse of 1Gy and 20 Gy at time $t = 360$ min and application of $1\mu\text{M}$ Nu7441.

time [min]	rep. 1
0	0
35.0000	0.9234
370.0000	1.2692

Data Set for Optimal Design \mathbf{D}_{II}^* The data set represents time course data of γH2AX for the optimized double pulse of 1 Gy at time $t = 0$ min and 20 Gy at time $t = 360$ min, both at a dose rates of 3.332 Gy/min and additional of (i) Nu7441 or Ku55933 or (ii) Nu7441 and Ku55933, including repetitions.

Supplementary Table 10: Part of processed data set including repetitions for γH2AX in arbitrary units for the optimized design \mathbf{D}_{II}^* and application of $1\mu\text{M}$ Ku55933.

time [min]	replicate 1	replicate 2	mean	variance
0	0	0	0	0
15.0000	0.3000	0.2700	0.2850	0.0004
35.0000	0.0100	0.3300	0.1700	0.0512
60.0000	-0.0800	0.3300	0.1250	0.0841
160.0000	-0.1000	0.2300	0.0650	0.0545
240.0000	-0.2800	0.3900	0.0550	0.2245
370.0000	0.8900	0.9500	0.9200	0.0018
420.0000	0.8400	0.7700	0.8050	0.0024
450.0000	0.5300	0.5200	0.5250	0.0001

Supplementary Table 11: Part of processed data set including repetitions for γH2AX in arbitrary units for the optimized design \mathbf{D}_{II}^* and application of $1\mu\text{M}$ Nu7441.

time [min]	rep. 1	rep. 2	rep. 3	rep. 4	mean	variance
0	0	0	0	0	0	0
15.0000	0.3700	0.1900	0.4500	0.2100	0.3050	0.0158
35.0000	0.6800	0.3400	0.2500	0.2300	0.3750	0.0436
60.0000	0.5800	-0.4200	0.2500	0.0500	0.1150	0.1750
160.0000	0.4100	-0.6800	-0.0100	-0.1600	-0.1100	0.2026
240.0000	0.4400	0.3400	0.2100	-0.0700	0.2300	0.0489
370.0000	1.5200	1.2300	1.3900	0.7700	1.2275	0.1071
420.0000	1.4100	1.1300	1.6300	0.6100	1.1950	0.1940
450.0000	0.9800	0.7800	1.3000	0.4800	0.8850	0.1188

Supplementary Table 12: Part of processed data set including repetitions for γ H2AX in arbitrary units for the optimized design \mathbf{D}_{II}^* and application of $1\mu\text{M}$ of Nu7441 and Ku55933.

time [min]	rep. 1	rep. 2	rep. 3	rep. 4	mean	variance
0	0	0	0	0	0	0
15.0000	0.1119	0.0506	0.2943	0.4913	0.2370	0.0394
35.0000	0.2939	0.1965	0.0905	0.6053	0.2966	0.0493
60.0000	0.0471	0.1236	0.0536	0.4099	0.1586	0.0293
160.0000	0.1789	0.1765	0.0223	0.2594	0.1593	0.0098
240.0000	-0.1896	0.1048	-0.0220	0.2791	0.0431	0.0393
370.0000	0.3661	0.7154	0.4716	0.8790	0.6080	0.0540
420.0000	0.1236	0.6413	0.4935	0.6847	0.4858	0.0650
450.0000	0.0028	0.4965	0.4070	0.5080	0.3536	0.0567

References

- Julie Bachmann, Andreas Raue, Marcel Schilling, Martin Boehm, Clemens Kreutz, Martin Bhm, Daniel Kaschek, Hauke Busch, Norbert Gretz, Wolf Lehmann, Jens Timmer, and Ursula Klingmueller. Division of labor by dual feedback regulators controls jak2/stat5 signaling over broad ligand range. *Molecular Systems Biology*, 7:516, 2011. ISSN 1744-4292.
- I. Brandsma and D. C. Gent. Pathway choice in dna double strand break repair: observations of a balancing act. *Genome Integr*, 3(1):9, 2012.
- C. E. Canman, D. S. Lim, K. A. Cimprich, Y. Taya, K. Tamai, K. Sakaguchi, E. Appella, M. B. Kastan, and J. D. Siliciano. Activation of the atm kinase by ionizing radiation and phosphorylation of p53. *Science*, 281(5383):1677–9, 1998.
- Doug W. Chan, Benjamin Ping-Chi Chen, Sheela Prithivirajasingh, Akihiro Kurimasa, Michael D. Story, Jun Qin, and David J. Chen. Autophosphorylation of the dna-dependent protein kinase catalytic subunit is required for rejoining of dna double-strand breaks. *Genes Development*, 16(18):2333–2338, 2002.
- Benjamin P. C. Chen, Naoya Uematsu, Junya Kobayashi, Yaniv Lerenthal, Andrea Krempler, Hirohiko Yajima, Markus Lbrich, Yosef Shiloh, and David J. Chen. Ataxia telangiectasia mutated (atm) is essential for dna-pkcs phosphorylations at the thr-2609 cluster upon dna double strand break. *Journal of Biological Chemistry*, 282(9):6582–6587, 2007.
- F. A. Cucinotta, J. M. Pluth, J. A. Anderson, J. V. Harper, and P. O’Neill. Biochemical kinetics model of dsb repair and induction of gamma-h2ax foci by non-homologous end joining. *Radiat. Res.*, 169(2):214–22, 2008.
- Xiaoping Cui, Yaping Yu, Shikha Gupta, Young-Moon Cho, Susan P. Lees-Miller, and Katheryn Meek. Autophosphorylation of dna-dependent protein kinase regulates dna end processing and may also alter double-strand break repair pathway choice. *Molecular and Cellular Biology*, 25(24):10842–10852, 2005.
- David O. Ferguson, JoAnn M. Sekiguchi, Sandy Chang, Karen M. Frank, Yijie Gao, Ronald A. DePinho, and Frederick W. Alt. The nonhomologous end-joining pathway of dna repair is required for genomic stability and the suppression of translocations. *Proceedings of the National Academy of Sciences*, 97(12):6630–6633, 2000.
- Ryan N. Gutenkunst, Joshua J. Waterfall, Fergal P. Casey, Kevin S. Brown, Christopher R. Myers, and James P. Sethna. Universally sloppy parameter sensitivities in systems biology models. *PLoS Comput Biol*, 3(10):e189, 2007.
- Alan C. Hindmarsh, Peter N. Brown, Keith E. Grant, Steven L. Lee, Radu Serban, Dan E. Shumaker, and Carol S. Woodward. SUNDIALS: Suite of nonlinear and differential/algebraic equation solvers. *ACM Trans. Math. Softw.*, 31(3):363–396, September 2005. ISSN 0098-3500. doi: 10.1145/1089014.1089020.

- G. S. Jimenez, F. Bryntesson, M. I. Torres-Arzayus, A. Priestley, M. Beeche, S. Saito, K. Sakaguchi, E. Appella, P. A. Jeggo, G. E. Taccioli, G. M. Wahl, and M. Hubank. Dna-dependent protein kinase is not required for the p53-dependent response to dna damage. *Nature*, 400(6739):81–3, 1999.
- Sabrina Koecher, Thorsten Rieckmann, Gabor Rohaly, Wael Y. Mansour, Ekkehard Dikomey, Irena Dornreiter, and Jochen Dahm-Daphi. Radiation-induced double-strand breaks require atm but not artemis for homologous recombination during s-phase. *Nucleic Acids Research*, 2012.
- C. Kreutz, M. M. Bartolome Rodriguez, T. Maiwald, M. Seidl, H. E. Blum, L. Mohr, and J. Timmer. An error model for protein quantification. *Bioinformatics*, 23(20):2747–2753, 2007.
- S. P. Lees-Miller, K. Sakaguchi, S. J. Ullrich, E. Appella, and C. W. Anderson. Human dna-activated protein kinase phosphorylates serines 15 and 37 in the amino-terminal transactivation domain of human p53. *Molecular and Cellular Biology*, 12(11):5041–9, 1992.
- Eckhard Limpert, Werner A. Stahel, and Markus Abbt. Log-normal distributions across the sciences: Keys and clues. *BioScience*, 51(5):341–352, 2001.
- Marta Martin, Anna Genesca, Laura Latre, Isabel Jaco, Guillermo E. Taccioli, Josep Egozcue, Maria A. Blasco, George Iliakis, and Laura Tusell. Postreplicative joining of dna double-strand breaks causes genomic instability in dna-pkcsdeficient mouse embryonic fibroblasts. *Cancer Research*, 65(22):10223–10232, 2005.
- Ciaran Morrison, Eiichiro Sonoda, Noriaki Takao, Akira Shinohara, Ken-ichi Yamamoto, and Shunichi Takeda. The controlling role of atm in homologous recombinational repair of dna damage. *EMBO Journal*, 19(3):463–471, 2000.
- Kazunari Mouri, Jose C. Nacher, and Tatsuya Akutsu. A mathematical model for the detection mechanism of dna double-strand breaks depending on autophosphorylation of atm. *PLoS ONE*, 4(4):e5131–, 2009.
- Jessica A. Neal and Katheryn Meek. Choosing the right path: Does dna-pk help make the decision? *Mutation Research/Fundamental and Molecular Mechanisms of Mutagenesis*, 711(12):73–86, 2011.
- A Raue, C Kreutz, T Maiwald, J Bachmann, M Schilling, U Klingmueller, and J Timmer. Structural and practical identifiability analysis of partially observed dynamical models by exploiting the profile likelihood. *Bioinformatics*, 25(15):1923–9, 2009. ISSN 1367-4803.
- Caroline A. Schneider, Wayne S. Rasband, and Kevin W. Eliceiri. Nih image to imagej: 25 years of image analysis. *Nat Meth*, 9(7):671–675, 2012.

Sheau-Yann Shieh, Masako Ikeda, Yoichi Taya, and Carol Prives. Dna damage-induced phosphorylation of p53 alleviates inhibition by mdm2. *Cell*, 91(3):325–334, 1997.

Meena Shrivastav, Cheryl A. Miller, Leyma P. De Haro, Stephen T. Durant, Benjamin P. C. Chen, David J. Chen, and Jac A. Nickoloff. Dna-pkcs and atm co-regulate dna double-strand break repair. *DNA Repair*, 8(8):920–929, 2009.